DOI 10.5012/bkcs.2011.32.6.2113

Experimental Analyses on Contrast Behaviors of iDQC and iTQC MR Images at 4.7 T

Jee-Hyun Cho,[†,‡] Janggeun Cho,[†,‡] Kee-Choo Chung,[†] Hyo-Yeon Yu,[†] Eun Kyung Ryu,[‡] Sangdoo Ahn,[†,*] and Chulhyun Lee[‡,*]

[†]*Department of Chemistry, Chung-Ang University, Seoul 156-756, Korea. [*]E-mail: sangdoo@cau.ac.kr*
[‡]*Division of Magnetic Resonance Research, Korea Basic Science Institute, Ochang, Cheongwon, Chungbuk 363-883, Korea [*]E-mail: chulhyun@kbsi.re.kr*
Received March 30, 2011, Accepted May 3, 2011

Key Words : Intermolecular multiple-quantum coherence, MRI, Contrast, iDQC, iTQC

Contrast in magnetic resonance imaging (MRI) is generally affected by the spin density, magnetic susceptibility, molecular diffusion, perfusion, and relaxation times (T_1 and T_2). Particularly, the relaxation times are the most dominant and controllable contrast-determining parameters in conventional MRI methods. Hence, many studies have been conducted on the development of contrast agents having the ability to change the T_1 and/or T_2 relaxation times to enhance the image contrast.[1-3] To create different contrasts compared to the conventional techniques, new imaging techniques have also been developed.[4,5] A new type of MR technique based on detecting *inter*molecular multiple quantum coherences (iMQCs) has recently attracted considerable attention, since it has the potential to provide a fundamentally different contrast mechanism from conventional MRI, because of the intrinsic sensitivity of the iMQCs to changes in the magnetization and susceptibility structures.[5-9]

In recent years, the feasibility and applications of intermolecular zero- and double-quantum coherences (iZQCs and iDQCs, second order iMQCs, respectively), in both *in vitro* and *in vivo* MRI, have been demonstrated with various samples.[5-9] The iZQCs and iDQCs correspond to simultaneously flipping two nuclear spins in the opposite and same directions on distant molecules, respectively. On the other hand, higher-order iMQCs, such as intermolecular triple-quantum coherences (iTQCs), have been rarely studied, because of their signal intensity limitations.[6] Nevertheless, iTQCs imaging could be more sensitive to the concentration and molecular motion, since they originate from distant dipolar interactions among three spins in separate molecules. Recently, the feasibility of iTQCs microscopic MR imaging in a high field micro-imaging system (14 T) was demonstrated.[6] Note that there have been some applications using the relatively strong MR signals from the *intra*molecular triple-quantum coherences of sodium, which has a 3/2 spin quantum number allowing for triple quantum jumps within an atom.[11]

In this study, we systematically analyzed the contrast behaviors of iDQCs and iTQCs MR images by comparing them with various conventional MR images obtained from echo planar imaging (EPI), T_2-weighted spin echo imaging (SE_T_2), T_2^*-weighted gradient echo imaging (GE_T_2^*), and T_1-weighted spin echo imaging (SE_T_1) techniques at 4.7 T. As shown in previous studies and theoretical expectations, the intensity profiles of the iMQCs with the echo time (TE) should be quite different from those of conventional MR images.[6,8,12-14] Thus, understanding the contrast characteristics of iMQCs MR images might be necessary, in order to utilize this technique effectively on many realistic applications, such as *in vivo* MRI for diagnosing diseases.

There are two different theoretical models used for explaining the effects of the dipolar interactions between spins on different molecules in solution.[15-17] One model treats the interaction classically using the Bloch equations modified to include the distant dipolar field (DDF) (or dipolar demagnetizing field) as a mean field. The DDF at a certain position is the overall sum of the local fields created by all of the spins in the sample. Thus, this field should depend on the spin distribution around; it could be negligible if the spin distribution is isotropic or symmetrical, while it becomes significant if the isotropy of the spin distribution is broken (e.g. by applying a field gradient pulse). It is also possible to treat the effects quantum mechanically by the spin density matrix formalism retaining the individual dipolar couplings explicitly and discarding the high-temperature approximation. This treatment clearly shows that the high-order terms in the spin density matrix are the origin of the iMQCs and could be converted into observable terms by the dipolar couplings.

A CRAZED type iMQC MR imaging pulse sequence, consisting of two *rf*-pulses and two field gradient pulses for the excitation and selection of the coherences, is depicted in Figure 1.[6,8,13] Two correlation gradients along the *z*-direction were used to select the iMQCs; the length of the second correlation gradient was twice or three times that of the first one. A traditional MR treatment would predict no signal, since there are no magnetizations doubly and/or triply modulated in spatial after the first *rf*-pulse. However, the intermolecular dipolar couplings between distant spins can convert the multi-spin terms (which were normally neglected) in the equilibrium density matrix into transverse magnetizations, hence producing signals. These signals arise from multiple nuclear spins separated around the correlation distance, $d = \pi/(\gamma GT)$, therefore the iMQCs MR images have the potential to reflect structural or dynamic variations on the distance scale.[6,8]

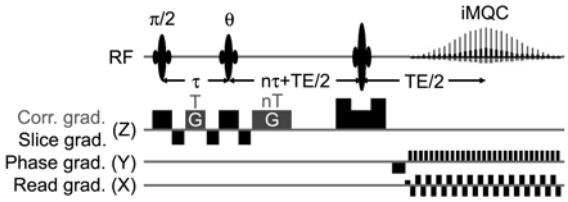

Figure 1. Pulse sequence for acquiring iMQCs MR images with the EPI readout.

Ignoring other dynamics such as relaxations, the signal at the echo time (TE) obtained from either the quantum or classical treatment is;[15]

$$M^{+} = i^{n-1} M_0 n\left(\frac{\tau_d}{\Delta_s TE}\right) J_n\left(-\frac{\Delta_s TE}{\tau_d}\right);$$

$$\Delta_s = \frac{\{3(\hat{s}\cdot\hat{z})^2 - 1\}}{2};\quad \tau_d = (\gamma\mu_0 M_0)^{-1} \qquad (1)$$

where J_n is the n^{th}-order Bessel function, s is the direction of the correlation gradient and τ_d is the dipolar demagnetizing time (~200 ms for pure water at room temperature in a 4.7 T magnet). This signal could be substantial; for example, the iDQC (n = 2) signal reaches a maximum at TE ~2.2τ_d, which corresponds to 36% of the single quantum magnetization. However, in most realistic imaging applications, spin relaxations make such a long TE impractical, hence the iMQC image signals should be weaker than those of conventional images. Therefore, the real utility of the iMQC images is expected to come from their different contrasts.

Figure 2 presents the MR images for a sample consisting of three parts having different $CuSO_4$ (as a contrast agent) contents in water, resulting in different T_1 and T_2 values. The relaxation times were calculated by using the series of SE_T_1 images and SE_T_2 images shown in the figure. The resulting images show that the relative contrasts among the three parts in the sample vary widely with the imaging technique and/or experimental conditions. Especially, the iDQC and iTQC images exhibit more strongly enhanced image contrasts among the three parts compared with the other conventional MR images under most experimental conditions.

Figure 3(a) shows the intensity profile of each part in the images in Figure 2. Note that the receiver gains were set differently for each imaging method to obtain good images. Additionally, the images have different intrinsic signal intensities depending on the imaging scheme, thus it is meaningless to directly compare the absolute intensities of these images. Therefore, to compare the image contrasts obtained using the different imaging methods, we used the signal intensities normalized to the maximum signal intensity (S/S_{max}) in the series of images obtained using each imaging method. The normalized signal intensity enables the image contrasts obtained using the different methods to be compared. As can be seen in Figure 3, the iDQC and iTQC MR imaging techniques with favorable experimental conditions enhanced the image contrasts dramatically.

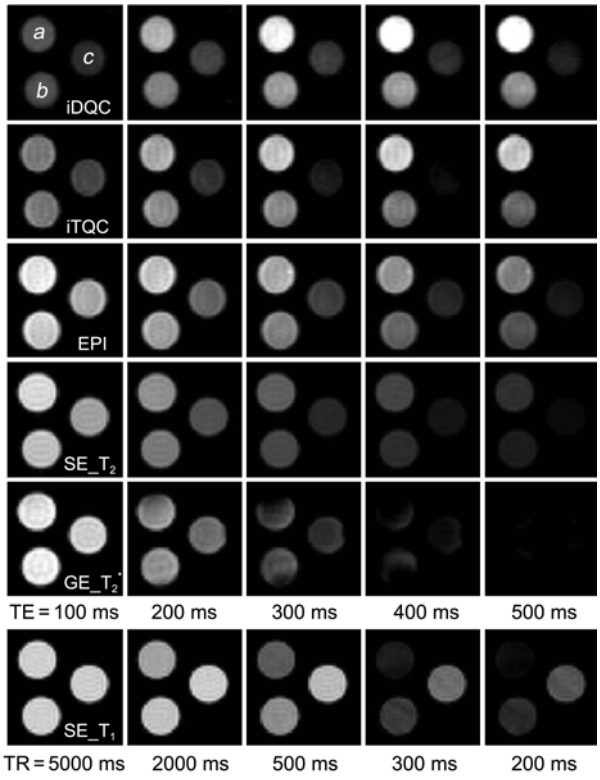

Figure 2. The MR images for the three parts having different $CuSO_4$ contents (*a*: 0.25 g/L $CuSO_4$, *b*: 0.50 g/L $CuSO_4$, and *c*: 1.00 g/L $CuSO_4$ aqueous solution) acquired with TE (or TR for SE_T_1) variation.

The fractional signal difference ($\Delta S/S_{max}$) was calculated to quantitatively assess the signal difference between the different parts of the images (see Figure 3(b)). Here, ΔS means the signal difference ($|S_i - S_c|$) between each part (S_i, i = *a*, *b* or *c*) and part *c* (S_c) which has the lowest signal intensity. This fractional signal difference represents the degree of image contrast for the different parts in one image which was acquired under the given experimental conditions, such as the imaging method, TR, TE, slice thickness and so on.

From Figure 3(b), it was found that the largest fractional signal difference in the iDQC or iTQC images is about 2-10 times higher than that in the EPI, SE_T_2, GE_T_2^* and SE_T_1 images. As described earlier, each part contains different amounts of contrast agent and, consequently, has different T_1 and T_2 values, while the spin densities are identical. Therefore, in the conventional imaging methods used in this experiment, the variations of T_1 and T_2 should be the only source of the contrast. Fundamentally, the image contrast in the iMQC MR imaging techniques is also significantly affected by the variation of the relaxation times, which is mainly associated with the changes in susceptibility. However, the signal characteristics in the iMQC MR imaging methods are quite different from those in the conventional T_2- and/or T_1-weighted MR methods, which could lead to the enhancement of the contrast. As one can easily see in Figures 2 and 3, the most striking difference is that the iMQC signals increase with increasing TE value, while the

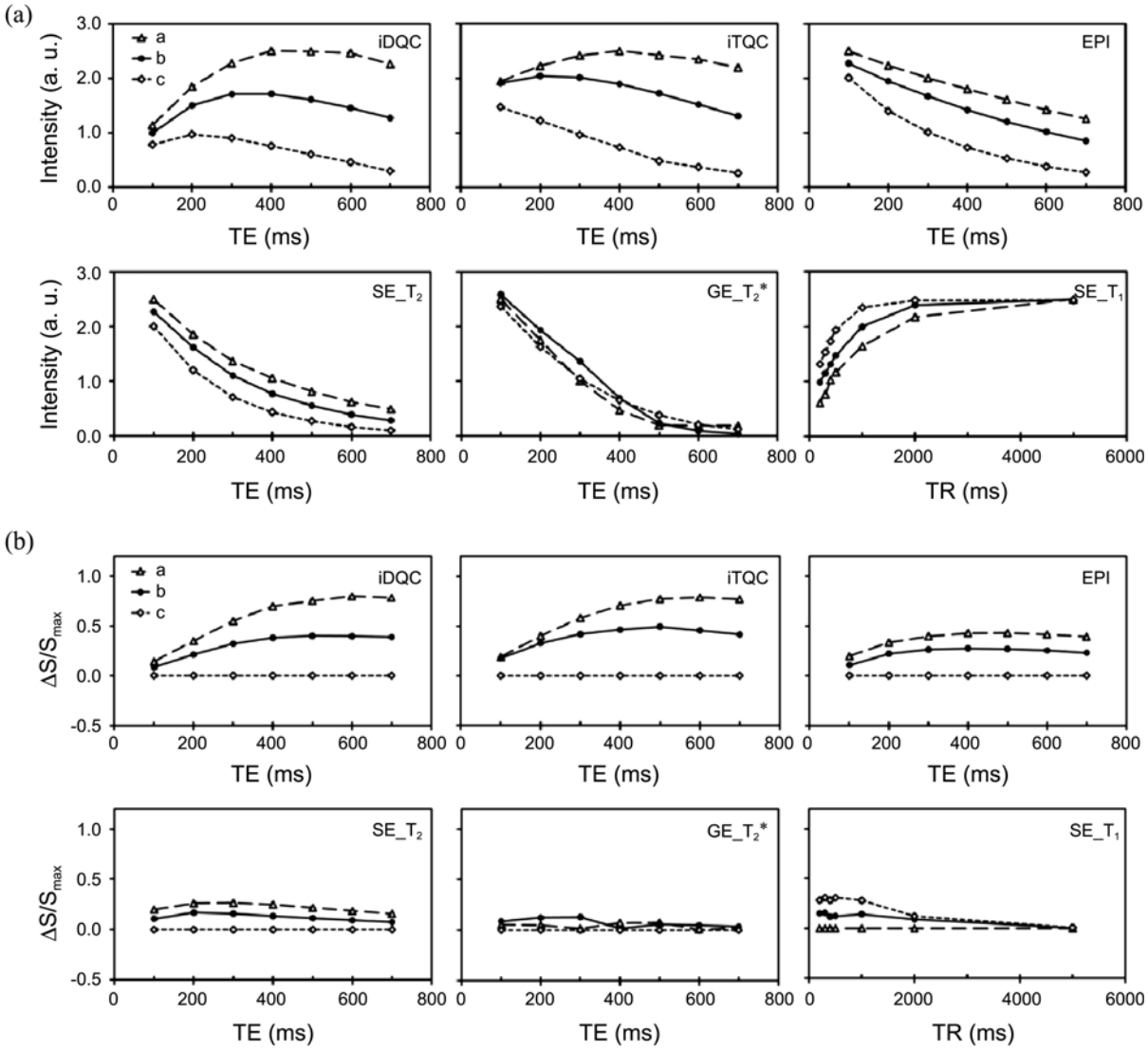

Figure 3. (a) The image intensity profiles and (b) the graphs of their calculated fractional signal difference ($\Delta S/S_{max}$) taken as a function of the TE (or TR for SE_T_1).

conventional MR signals just decay. It takes time to render the iMQCs observable (converting the iMQCs into single quantum coherences by the intermolecular dipolar couplings). There is a competition between the signal growing and decaying dynamics, which correspond to the intermolecular dipolar couplings and relaxation processes, respectively. Therefore, the maximum point is definitely controlled by the relaxation times, T_1 and T_2. Especially, the effects of the variations of the relaxation time on the signal intensities are magnified in the iMQCs, since they come from multi-spin interactions (e.g. $I_i^+ I_j^+$ for iDQCs) influenced by multi-exponential decaying with the relaxation times of the individual spins.[18] For part *a* (having the longest T_1 and T_2), the signal intensity of the iMQC images continuously increases up to a TE of ~500 ms, and then starts decaying slowly (see Figure 3(a)). For part *c*, the maximum of the iDQC signals is reached at a TE of ~200 ms and the intensity is approximately 1/2 or 1/3 of the signal of part a at 200 ms or the maximum point, respectively. As a result, the image contrast between each part in the iMQC increases with increasing TE. On the other hand, as the TE is increased, the signal intensity of each part in the conventional MR imaging methods, such as the T_2-weighted techniques, simply decays exponentially in proportion to the relaxation rate ($1/T_2$) of each part. Thus, the difference in image contrast between the iMQC and conventional methods is relatively small at short TEs, but it becomes significantly enlarged as the TE is increased (see Figure 3(b)).

Compared with the iDQC MR images, the high-order iMQCs (such as iTQCs) images were not studied extensively, due to the relatively weak signals associated with the number of spins involved in the creation of the coherences. However, as shown in the previous study, high coherence order iMQC MR imaging could be very useful for the investigation of small heterogeneity in samples (e.g. spin density, relaxation times, structural defects, etc.) at a high magnetic field.[6] Fundamentally, the effects of the heterogeneity in multispin interactions would be amplified as the

order is increased at the expense of the signal intensity of the image. At a low magnetic field and/or low spin density, the signal build up time is too long to overcome the signal decay due to the relaxation process. Nevertheless, it intrinsically has the uniqueness and effectiveness in contrast enhancement which makes it worthwhile studying in depth. In this experiment, as shown in Figure 3, the feasibility and utility of iTQCs MR imaging for contrast enhancement were also demonstrated at 4.7 T with favorable experimental conditions.

In summary, we demonstrated that the iDQC and iTQC MR images are readily observable on a 4.7 T animal scanner. The systematical analyses of the contrast behaviors of these images, reflecting the differences in the relaxation times (T_1 and T_2), show that they have unique and significantly enhanced contrast compared with the images obtained from the various conventional MR imaging methods.

Experimental Section

Sample Preparations. We used three solutions which have different T_1 and T_2 relaxation times. They are H_2O solutions including 1.00 g/L $CuSO_4$ (T_1/T_2 = 201/176 ms), 0.50 g/L $CuSO_4$ (T_1/T_2 = 454/245 ms) and 0.25 g/L $CuSO_4$ (T_1/T_2 = 737/334 ms). Each solution was put in a regular 5-mm *o.d.* NMR tube, and the three solution tubes were put in a 15 mL conical tube containing the D_2O solution.

MRI Measurements. All MRI experiments were performed on a 4.7 T animal MRI scanner (BioSpec 47/40; Bruker, Germany) with a 35 mm volume coil at KBSI in Ochang. The experimental data were obtained and analyzed in ParaVision 4.0 (Bruker, Germany). All iMQC images were acquired with the CRAZED-type pulse that includes the echo planar imaging (EPI) readout in *k*-space. We also obtained the conventional SE-EPI, SE-T_1, SE-T_2, GE-T_2^* images to compare their contrast with that of the iMQC images. To acquire all of the images, we used the following parameter settings: field of view (FOV) = 19.2 × 19.2 mm^2, slice thickness = 1 mm and matrix size = 64 × 64. We set the repetition time (TR) to ~5 s except for the T_2^* images (TR = 1 s) to minimize contamination from stimulated or inter-scan stimulated echoes. We obtained the images with various contrasts by varying some of the experimental conditions (TE or TR). For the iMQC images, we set the correlation distance to 600 μm.

Acknowledgments. This work was supported by the Ministry of Education, Science and Technology, Republic of Korea (2010) ("The Support Program for the Advancement of National Research Facilities and Equipment"). The authors wish to thank the KBSI for the operation of the 4.7 T MRI and 14 T microscopic MRI. This work was also supported by the Korea Basic Science Institute Grant (T31404) and NAP of the Korean Research Council of Fundamental Science & Technology (PGA061).

References

1. Kirsch, J. E. *Top. Magn. Reson. Imaging* **1991**, *3*, 1.
2. Burtea, C.; Laurent, S. L.; Elst, V.; Muller, R. N. *Handbook of Experimental Pharmacology* **2008**; pp 135-165.
3. Kim, D.; Kim, J. W.; Jeong, Y. Y.; Jin, S. *Bull. Korean Chem. Soc.* **2009**, *30*, 1855.
4. Huang, S. Y.; Wolahan, S. M.; Mathern, G. W.; Chute, D. J.; Akhtari, M.; Nguyen, S. T.; Huynh, M. N.; Salamon, N.; Lin, Y. Y. *Magn. Reson. Med.* **2006**, *56*, 776.
5. Zhang, S.; Zhu, X.; Chen, Z.; Cai, C.; Lin, T.; Zhong, J. *Phys. Med. Biol.* **2008**, *53*, N287.
6. Cho, J. H.; Ahn, S.; Lee, C.; Hong, K. S.; Chung, K.-C.; Chang, S.-K.; Cheong, C.; Warren, W. S. *Magn. Reson. Imaging* **2007**, *25*, 626.
7. Shannon, K. L.; Branca, R. T.; Galiana, G.; Cenzano, S.; Bouchard, L. S.; Soboyejo, W.; Warren, W. S.; *Magn. Reson. Imaging* **2004**, *22*, 1407.
8. Warren, W. S.; Ahn, S.; Mescher, M.; Garwood, M.; Ugurbil, K.; Richter, W.; Rizi, R. R.; Hopkins, J.; Leigh, J. S. *Science* **1998**, *281*, 247.
9. Marques, J. P.; Bowtell, R. *Magn. Reson. Med.* **2004**, *51*, 148.
10. Zhong, J.; Chen, Z.; Kwok, E. *Magn. Reson. Med.* **2000**, *43*, 335.
11. Borthakur, A.; Hancu, I.; Boada, F. E.; Shen, G. X.; Shapiro, E. M.; Reddy, R. *J. Magn. Reson.* **1999**, *141*, 286.
12. Enss, T.; Ahn, S.; Warren, W. S. *Chem. Phys. Lett*. **1999**, *305*, 101.
13. Rizi, R. R.; Ahn, S.; Alsop, D. C.; Garrett-Roe, S.; Scgnall, M. D.; Leigh, J. S.; Warren, W. S. *Magn. Reson. Med.* **2000**, *43*, 627.
14. Bouchard, L.-S.; Rizi, R. R.; Warren, W. S. *Magn. Reson. Med.* **2002**, *48*, 973.
15. Lee, S.; Richter, W.; Vathyam, S.; Warren, W. S. *J. Chem. Phys.* **1996**, *105*, 874.
16. Ahn, S.; Warren, W. S.; Lee, S. *J. Mag. Reson*. **1997**, *128*, 114.
17. Warren, W. S.; Lee, S.; Richter, W.; Vathyam, S. *Chem. Phys. Lett*. **1995**, *247*, 207.
18. Warren, W. S.; Ahn, S. *J. Chem. Phys*. **1998**, *108*, 1013.